JPEDAV (2007) 28:150–157
DOI: 10.1007/s11669-007-9023-z
1547-7037 ©ASM International

Thermodynamics of the Au-Si-O System: Application to the Synthesis and Growth of Silicon-Silicon dioxide Nanowires

Djamila Bahloul-Hourlier and Pierre Perrot

(Submitted September 19, 2005)

The Solid-Vapor-Liquid-Solid (SVLS) process is a fundamental mechanism for the growth of nanowires. In this article, experimental observations and assessment of thermodynamic data have been used to explain the Solid-Vapor-Liquid-Solid (SVLS) mechanism for the growth of silicon-based nanowires. The binary phase diagram of nanoparticle (Au-Si) systems has been evaluated from information on Gibbs energy of the bulk and surface tension of the liquid phase. At 1100 °C, temperature commonly used for the growth of nanowires by the SVLS mechanism, it has been shown that the nanometric decreases the melting point of pure Au and Si and more generally the liquidus temperatures. Moreover, the liquid phase region in the binary Au-Si phase diagram is enlarged as the particle size becomes smaller. The presence of SiO in the gaseous phase is a necessary but not sufficient condition for the formation of nanowires. The nanowires'growth cannot be explained by the modification of the Au-Si phase diagram with the size of the particles, neither by the presence of SiO, but by the existence of a metastable equilibrium involving the silicon of the wafer, the deposit of vitreous silica and supersaturated SiO in the gaseous phase.

Keywords binary system Au-Si, nanodiagrams, nanowhiskers, S(V)LS mechanism, thermodynamics

1. Introduction

Nanowires have been gaining a lot of attention recently as alternatives to carbon nanotubes (CNT), because their growth and doping with suitable impurities are relatively easier to control. Many successful synthetic strategies have been developed to obtain bulk quantities of nanowires, using both gas phase and condensed phase techniques. Thus, a broad range of multicomponent semiconductor nanowires has been explored using various methods including the vapor-phase transport process,[1] chemical vapor deposition,[2,3] arc discharge,[4] laser ablation,[5] solution,[6], and a template-based method.[1] Silicon nanowires (SiNWs) are particularly attractive due to the central role of the silicon semiconductor industry for potential nanotechnology applications. The growth mechanism of silicon nanowires in these techniques is commonly explained either by the vapor-liquid-solid (VLS) or solid-liquid-solid (SLS) growth models.

Djamila Bahloul-Hourlier, Institut d'Electronique, de Microélectronique et de Nanotechnologies, UMR-CNRS 8520, F-59652 Villeneuve d'Ascq, France; **Pierre Perrot,** Laboratoire de Métallurgie Physique et Génie des Matériaux, UMR-CNRS 8517, Université des Sciences et Technologies de Lille, F-59655 Villeneuve d'Ascq, France. Contact e-mail: djamila.hourlier@isen.iemn.univ-lille1.fr

The vapor-liquid-solid (VLS) mechanism was first suggested by Wagner and Ellis [7] who showed that micrometer-scale silicon whiskers (wires) could be grown from metal-droplet catalysts under Chemical Vapor Deposition (CVD) conditions at about 1000 °C. The process was named the "Vapor-Liquid-Solid" (VLS) mechanism after the three phases involved. VLS growth was extended to micrometer-scale whiskers of many inorganic materials such as SiC, Si_3N_4, and intensively studied for over a decade as reinforcement in matrix composites, before fading into relative obscurity.

In the vapor-liquid-solid (VLS) crystal growth mechanism, the vapor phase is supplied in the form of volatile species issued from gaseous precursors (SiH_4, $SiCl_4$ ...), liquid precursors (MOCVD), or by thermal decomposition of solid. Gold is the most favorable catalyst for low-temperature synthesis from its binary diagram, because (Au/Si) alloy liquid phase presents a deep eutectic at about 360 °C. The liquid nanosized droplet on the surface of a substrate acts as the preferential site for absorption of gas-phase reactant and, when supersaturated, as a very convenient nucleation site for growth. Nanowire's growth continues as long as the reactant is available with the alloy droplet riding on top of the wire. As a result, the diameter of nanowires is comparable to that of the catalyst nanoparticle.

Many other researchers grew amorphous silicon nanowires by heating metal-coated silicon substrate at high temperature in an argon and hydrogen atmosphere. As, during this process, the silicon goes from the solid wafer to the liquid droplet and finally to solid nanowires form, it was termed a Solid-Liquid-Solid (SLS) mechanism of growth.

Yan et al.[8], Yu et al.[9], and Paulose et al.[10] postulated that the growth by the SLS mechanism occurred through silicon

diffusion from the substrate to the gold-silicon melt formed on the surface at high temperature. With time, more silicon, from the substrate, diffuses into the droplet, making it supersaturated with silicon and then the coexisting pure silicon phase precipitates and crystallizes as nanowires. This argument cannot be accepted as there is no thermodynamic (energetic) reason for the silicon of the wafer to supersaturate the binary liquid phase.

From a thermodynamic point of view, it is easy to accept the saturation of gold with silicon issued from the wafer by diffusion. However, once the saturation is obtained, the chemical potential of silicon in solid, liquid alloy (metal-Si), and gaseous phases is the same. Recently, some authors reported on the growth of nanowires by a process, which does not require any silicon-based vapor or metal catalysts. They suggested a stress-driven mechanism in which the stress gradient between the native oxide and the underlying Si wafer leads to the accumulation of silicon in crack regions and promote the growth of nanowires.[11,12]

Although substantial progress has been made in the production of nanometric materials since their discovery more than a decade ago, the SLS growth mechanism is still poorly understood. Thus, the purpose of the present work is to discuss from a thermodynamic point of view the growth of nanowires by the solid-liquid-solid (SLS) process and to point out the conditions in which nanowires can be obtained.

2. Experimental

The procedure of preparation employed has been previously detailed.[10] Briefly, a silicon wafer is recovered by oxidation with a thin layer of silicon dioxide (native oxide), and, by solid phase transportation, with a gold layer. The system is then heated at 1100 °C under an Ar-H_2 (3% H_2) atmosphere. As it melts, the gold layer gathers in the form of liquid droplets whose diameter lies between 25 and 100 nm.

The nanowires are observed to form in a few minutes. Their diameter has been measured to be in the 10-100 nm and their typical length is of the order of several μm . The morphology of nanowires, shown in Fig. 1(a), is characterized by the formation of a Si-SiO_2 composite (Fig. 1(b)). Our aim in this study is not to repeat the bulk synthesis of nanowires and their characterization but to discuss from a thermodynamic point of view the growth of nanowires by connecting the results of our own experiments and previously published results, and to point out the conditions in which nanowires can be obtained. We demonstrate that the so-called SLS process is actually a Solid-Vapor-Liquid-Solid (SVLS) process, owing to the fundamental role played by the gaseous phase in the nanowires' growth.

3. The Stable Au-Si-O Ternary System

The Au-Si-O diagram is important with respect to the vapor species in equilibrium with Au-Si liquid alloys.

3.1 Au-Si

The Au-Si assessed by Okamoto and Massalski[13] presents a deep eutectic, which is the indication of a strong

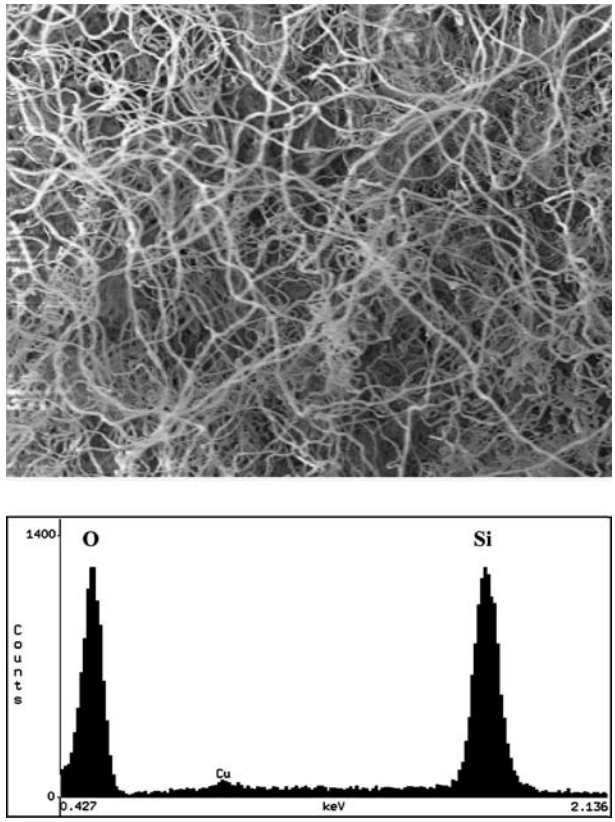

Fig. 1 (a) SEM micrograph showing the general morphology of SiNWs grown via a SLS mechanism at 1100 °C under Ar-3% H_2 atmospheres (b) EDX analysis.

attractive interaction between Au and Si in the liquid state, in contrast with the strong repulsive interaction between Au and Si in the solid state. Indeed, the eutectic temperature is experimentally measured at 363 °C whereas, in the hypothesis of an ideal liquid solution, the eutectic temperature would be calculated at 870 °C. The thermodynamic description of the liquid phase giving the best fit with experimental liquidus lines is the Redlich-Kister development proposed by Tanaka and Hara[14] and reproduced in Table 1. A metastable phase tentatively considered as Au_3Si has been synthesized by Saunders[16] with splat quenching alloys at cooling rates of $\approx 10^5$ K s^{-1}. Its structure is very complex and an estimation of its Gibbs energy is reported in Table 2. The formation of a gold film on Silicon NanoWire (SiNW) under the converging electron beam of a TEM has been explained by Teo[17] from the presence of metastable Au_3Si.

3.2 Au-O

The Au-O interactions are known to be very weak. The solubility of oxygen in liquid gold at 1550 °C was evaluated[18] between 1 and 2 ppm under 0.1 MPa of oxygen pressure.[18] Gold sesquioxide Au_2O_3, stable under oxygen pressures higher than 0.1 MPa, does not exist under our experimental conditions.

Table 1 Thermodynamic data of the Au-Si system

$G°(Au,L) - G°(Au,fcc) = 12\ 552 - 9.385\ 866T$ [15]
$G°(Si,L) - G°(Si,diamond) = 50\ 696.36 - 30.099\ 439\ T + 2.093\ 1\times10^{-21}T^7$[15]
$G°(Au_3Si, \textit{metastable}) = +2\ 750 + 3T$[16]
$G_L^{xs} = x(1-x)\sum L_i\ (1-2x)^i$ where x is the mole fraction of Si in the liquid alloy
$L_0 = -23\ 863.9 - 16.234\ 38\ T$
$L_1 = -20\ 529.55 - 6.039\ 58\ T$
$L_2 = -8\ 170.5 - 4.273\ 2\ T$
$L_3 = -33\ 138.25 + 26.566\ 65\ T$[14]

3.3 Si-O

The Si-O binary system has been extensively reviewed by,[19] which confirmed earlier work[20] and pointed out the fact that, gaseous species in equilibrium with condensed phases are mainly Si, Si_2, Si_3, O_2, O, SiO, Si_2O_2 and SiO_2, and then was thermodynamically assessed by Hallstedt[21]. A thorough investigation of[22] lead to the best available thermodynamic description to date. Under reducing conditions with Si present, SiO_2 vaporizes mainly by giving off SiO[23]. The condensation of SiO gives an amorphous phase whose stability at high temperature (above 1300 °C) is controversial. An Electron spectroscopic evidence[24] shows that amorphous SiO transforms to a microscopic mixture of Si + SiO_2 when increasing temperature above 500 °C. Vapor pressure measurements[25] carried out by means of a Knudsen cell show that amorphous SiO behaves as an equimolecular mixture Si + SiO_2. Chatillon et al.[26] using an equimolecular mixture Si + SiO_2 corresponding to the maximum rate of reaction, show that the main species present in the gaseous phase is SiO, followed by a very low partial pressure of Si_2O_2. In oxidizing conditions, SiO_2 predominates in gaseous species up to 1726 °C. In the solid phase, the Si-SiO_2 eutectic forms 0.4 °C below the melting point of silicon (1414 °C). The oxygen solubility (under $P_{O_2} = 1.06 \times 10^{-13}$ MPa which is the oxygen potential of the silicon-cristobalite equilibrium at the melting point of silicon) at the eutectic temperature is 0.0125 at.% (6×10^{18} atoms cm^{-3}) in the liquid phase and 0.00375 at.% (1.8×10^{18} atoms cm^{-3}) in the solid phase,[23], in fair agreement with calculations of [21].

Table 2 Molar volume V and surface tension σ of Au and Si around the melting point

Element	V/m^3 mol^{-1}	σ /J m^{-2}	$(\partial\sigma/\partial T)$/J m^{-2} K^{-1}
Au, cfc	10.76×10^{-6}[29]	1.46 (estimated)	-2.5×10^{-4}
Au, L	11.39×10^{-6}[29]	1.169[14]	-2.5×10^{-4}
Si, diamond	12.27×10^{-6} (calculated)	1.08 (estimated)	-1.3×10^{-4}
Si, L	11.10×10^{-6}[14]	0.865[14]	-1.3×10^{-4}
SiO_2, crist.	143×10^{-6} (calculated)	0.6[30]	

4. Growth of Nanowires

Four phases are present in the system: two solid phases, Si and SiO_2, which are in equilibrium with the gaseous phase whose main constituent is SiO under a pressure of 4.05 Pa at 1100 °C. The liquid phase, in contact with the solid and gaseous phases, has to be in equilibrium, and thus saturated with silicon. When the equilibrium is reached, the chemical potential of silicon is the same in every phase and no more driving force exists to justify the nanowire growth experimentally observed. The explanation of this process has to be found in the presence of metastable equilibria developed in the system. Two sources of metastability may be pointed out. The first one may come from the fact that the Au-Si phase diagram in the bulk state differs from the Au-Si phase diagram of nanometric particles. The second source of metastability may come from the fact that SiO_2 on the silicon wafer is amorphous silica rather than crystallized under the form of stable cristobalite. Therefore in this work these two potential sources of metastability have been examined.

4.1 The Au-Si Diagram of Nanoparticles

The mean radius of the system of interest is 25 nm, for the gold droplets as well as for the nanowires. The interfacial forces cannot be neglected, because the ratio surface/volume is of the order of $2/n$ for a cylinder, and $3/n$ for a sphere, n being the number of atoms along a radius. With a mean atomic diameter of 0.30 nm for liquid gold and 0.24 nm for silicon type diamond, it is easy to see that, 0.4% of the gold atoms are on the surface of the gold droplets, and 0.3% of the silicon atoms are on the surface of the nanowires. The influence of the surface energy although weak must be evaluated.

The Gibbs energy of the liquid droplet is the sum of two terms:

$$G_L = G_L^{bulk} + G_L^{surf}$$

$$G_L^{bulk} = xG^{\circ}_{Si,L} + (1-x)G^{\circ}_{Au,L} + RT[x\ln x + (1-x)\ln(1-x)] + G_L^{xs}$$

where x is the mole fraction of Si in the liquid droplet; $G°_{Si,\ L}$ and $G°_{Au,\ L}$, are the Gibbs energies of pure liquid Si and pure liquid Au, given in Table 1, and G_L^{xs} is the excess Gibbs energy of the liquid phase in the bulk given by the Redlich-Kister development shown in Table 1.

An expression of G_L^{surf}, the surface Gibbs energy of the liquid, has been proposed by:[27]

$$G_L^{surf} = 2\sigma_L V_L/r$$

where r is the radius of the particle, σ_L and V_L are surface tension and molar volume of the liquid alloy. The difference between molar volumes of pure liquid components being lower than 4%, the molar volume of the liquid alloy is given by a linear relationship:

$$V_L = (1-x)V_{Au,L} + xV_{Si,L}$$

σ_L is calculated from the Butler's equation as follows [14, 28]:

$$\sigma_L = \sigma_{Au,L} + (1/\Omega_{Au})\{R\,T\ln[(1-y)/(1-x)] + \mu_{Au}^{xs,surf}(T,y) - \mu_{Au}^{xs,bulk}(T,x)$$

$$\sigma_L = \sigma_{Si,L} + (1/\Omega_{Si})\{R\,T\ln(y/x) + \mu_{Si}^{xs,surf}(T,y) - \mu_{Si}^{xs,bulk}(T,x)\}$$

Here $\sigma_{X,L}$ (where X = Au, Si) is the surface tension of pure liquid element X given in Table 2. Ω_X is the molar surface of the liquid X given by $\Omega_X = bN_o^{1/3}V_X^{2/3}$, where N_o is the Avogadro number and b is a geometric factor (1.091 for a close packed lattice); x and y are respectively the mole fraction of Si in the bulk and on the surface; $\mu_X^{xs,bulk}(T,x)$ and $\mu_X^{xs,surf}(T,y)$ are the excess chemical potential of the element X in the bulk and on the surface respectively:

$$\mu_{Au}^{xs,bulk}(T,x) = G_L^{xs,bulk} - x(\partial G_L^{xs,bulk}/\partial x)$$

$$\mu_{Si}^{xs,bulk}(T,x) = G_L^{xs,bulk} + (1-x)(\partial G_L^{xs,bulk}/\partial x)$$

$\mu_{Au}^{xs,surf}(T,y)$ and $\mu_{Si}^{xs,surf}(T,y)$ are derived from the model proposed by Yeum et al.[28]

$\mu_X^{xs,surf}(T,x) = \beta\mu_X^{xs,bulk}(T,x)$ with X=Au or Si.

$\beta = 0.83$ for liquid metallic alloys is the parameter corresponding to the ratio of the coordination number in the surface to the coordination number in the bulk. Both expressions for σ_L form a system of two equations with two unknown parameters (σ_L and y) and may be used to derive $y(x)$, the surface composition versus the bulk composition, then derivation $\sigma_L(x)$ or $\sigma_L(y)$ follows. Figure 2 gives $\sigma_L(x)$ and $\sigma_L(y)$ for the Au-Si liquid alloy at 1100 °C, the temperature of interest. This figure allows deriving the relationship between $\sigma_L(x)$ and $\sigma_L(y)$. Whatever the composition of the bulk, the surface is always enriched in silicon. The surface tension of the liquid alloy presents a positive deviation from ideality, which correlates the attractive interaction between Au and Si in the liquid phase.

The Gibbs energy of a silicon nanowire is given by:

$$G_{Si,nano} = G_{Si}^{\circ\,bulk} + G_{Si}^{surf} = 2\,\sigma_{Si,S}\,V_{Si,S}\,/\,r$$

where $\sigma_{Si,S}$ and $V_{Si,S}$ are surface tension and molar volume of the pure solid Si, respectively, and are given in Table 2. $G_{Si}^{\circ bulk} = 0$ because pure Si diamond is selected as standard state.

The Gibbs energy of the liquid in the bulk at 1100 °C is compared with the Gibbs energy of the nanodroplets (5 nm of radius) in Fig. 3. With droplets of 25 nm of radius, the Gibbs energy of the bulk is lowered by a mean amount of 980 J.

From the curves $G_L = f(x, r, T)$, it is possible to calculate several nanodiagrams, with differences dependent on the size of the liquid droplet and the crystals in equilibrium with the liquid. For instance, the abscissa of the point s (56 at.% Si) and s' (60 at.% Si) in Fig. 3 represent the solubility of the Si wafer ($G_{Si}^{\circ\,bulk} = 0$) and the solubility of the Si nanocrystal ($G_{Si,nano} = 2\sigma_{Si,S}V_{Si,S}/r = 1354$ J mol^{-1} for r = 5nm) in the bulk liquid Au, respectively. The result is well known: the solubility of small particles in a given solvent is higher than the solubility of great particles. More interesting is the following result: if we compare the solubilities of liquid particles in liquid of various sizes, we observe that solubility decreases with the radius of the droplet. For instance, the solubility of a Si wafer is 56 at.% in bulk liquid Au, and only 51% in a liquid droplet whose radius is 5 nm. The nanometric phase diagram (crystals of radius 5 nm in equilibrium with droplets of radius 5 nm) compared with the phase diagram in the bulk presented in Fig. 4 shows an increase of the liquid domain in the nanodiagams.

In conclusion, the phase diagram of nanoparticles presents minute modifications for particles with 25 nm of radius, and more important modifications for particles with 5 nm of radius. The crystallization temperature of gold goes down from 1064 °C ($r = \infty$) to 1043 °C when r = 25 nm, and 962 °C when r = 5 nm. For silicon, the temperatures are respectively 1414 °C ($r = \infty$), 1405 °C (r = 25 nm), and 1365 °C (r = 5 nm).

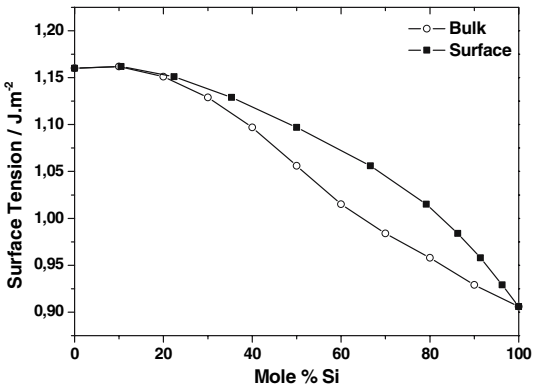

Fig. 2 Surface tension of liquid alloy in the bulk.

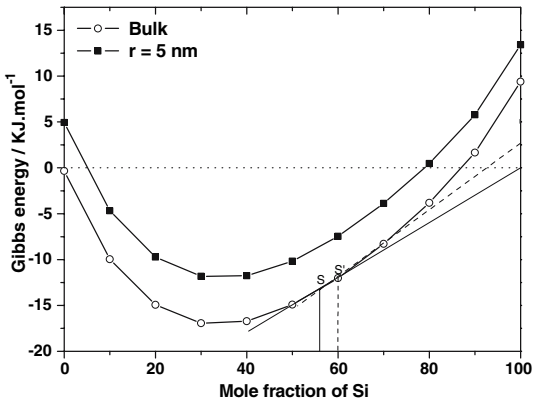

Fig. 3 Gibbs Energy of Au-Si liquid alloys at 1100°C for the bulk (r = ∞) and for droplets (r = 5 nm).

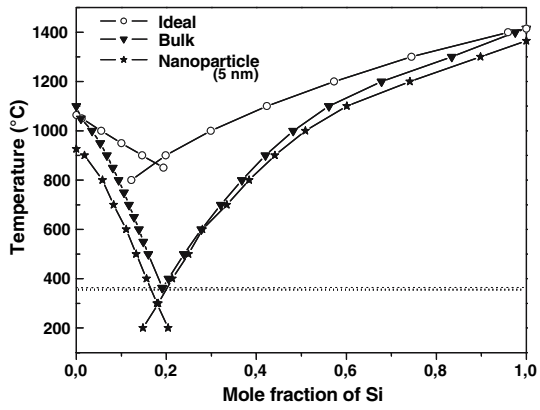

Fig. 4 Comparison of the Au-Si phase diagram for the bulk and for droplets (r = 5 nm) in equilibrium with nanocrystals (r = 5 nm).

4.2 The Au-Si-O Diagram of Nanoparticles

The main characteristics of the Au-Si-O phase diagram above 363 °C, the eutectic temperature of the Au-Si binary system, is the presence of a two phase field liquid alloy-silica. Each tieline is characterized by an oxygen potential and by a SiO potential in equilibrium with the Alloy-SiO_2 mixture. These potentials are governed by the following equilibria:

$$Si_{Au} + O_2 \rightarrow <SiO_2> \quad [1]$$
$$R\,T \ln (P_{O_2}/P^\circ) = \Delta_{r1}G^\circ - R\,T \ln (a_{Si}/a_{SiO_2})$$

$$1/2[Si]_{Au} + 1/2\langle SiO_2\rangle \rightarrow SiO \quad [2]$$
$$R\,T \ln (P_{SiO}/P^\circ) = -\Delta_{r2}G^\circ + 1/2R\,T \ln (a_{Si}a_{SiO_2})$$

The standard state for SiO_2 is solid cristobalite, which is the stable form of silica for the temperature range of interest. $[Si]_{Au}$ represents silicon dissolved in liquid Au. The standard state for Si is pure solid silicon whose crystal structure is that of C (diamond). The standard pressure for gaseous species (O_2 and SiO) is $P^\circ = 10^5$ Pa. Figure 5 shows the stable and metastable equilibria in the Au-Si-O diagram calculated at 1100 °C.

In the stable diagram, liquid Au saturated with silicon (56 at.%Si is in equilibrium with solid silicon and with solid silica under a SiO pressure of 4.05 Pa and an oxygen pressure of 4.52×10^{-21} Pa. In the metastable diagram, liquid Au supersaturated with silicon (60 at.%Si is in equilibrium with solid silicon and with solid silica under a SiO pressure of 4.56 Pa and an oxygen pressure of 5.73×10^{-21} Pa.

In the two-phase field, the oxygen pressure increases with the gold content of the alloy whereas the SiO pressure decreases with the silicon content of the alloy. The three phase field $[Si]_{Au}$–SiO_2–O_2 is not shown in Fig. 5 because its equilibrium identifies with the Au-O side of the triangle: under an oxygen pressure of 0.1 MPa, the activity of silicon in the liquid alloy in equilibrium with SiO_2 is $a_{Si} = 4.5\times10^{-26} \approx 0$. Beyond SiO and O_2, the main gaseous species in equilibrium with the condensed phases Si and SiO_2 are Si, Si_2, Si_3, and SiO_2. The partial pressures of these species, calculated between 700 and 1700 K with the ThermoCalc software are shown in Fig. 6.

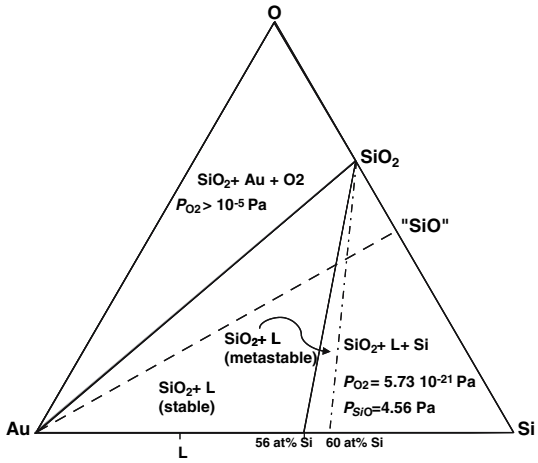

Fig. 5 Metastable Au-Si-O diagram at 1100°C.

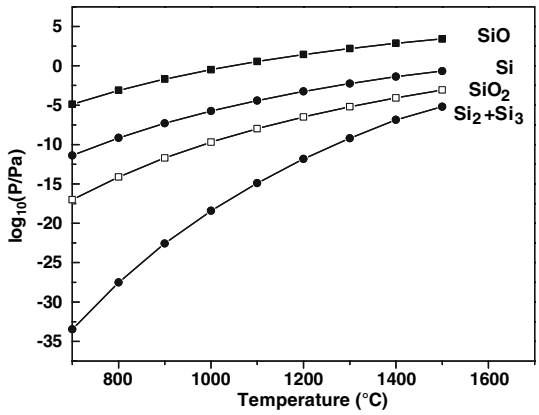

Fig. 6 Partial pressures of gaseous species in equilibrium with Si-SiO_2 cristobalite mixture.

4.3 Gas-Liquid Interaction

The modification of the Au-Si phase diagram, even if not dramatic, is however noticeable by taking into account the surface energies of the gold droplets and of the silicon nanowires. However, that modification cannot be the cause of the nanowires growth because the activity of Si in a liquid alloy in equilibrium with the wafer does not depend on the size of the droplet. An equilibrium between the three phases implies equality of the silicon chemical potential in the three phases, that is, an activity of the silicon equals to 1, because our choice of standard state is the solid silicon of the wafer. The liquid phase can be in equilibrium with the silicon of the wafer, but not with the silicon of a nanowire, in which $a_{Si} > 1$. At 1100 °C, by taking $a_{Si} = 1$ for the silicon of the wafer, it is easy to calculate $a_{Si} = 1.623$ for a particle of radius $r = 5$ nm. Once an equilibrium state is obtained, that is, once the gold droplets are saturated with silicon, there is no reason to observe the growth of nanowires, because the driving force needed to trigger the silicon precipitation does not exist. It is widely acknowledged that the first step of the process is the supersaturation of the gold droplet in silicon,

the second step being the germination and growth of nanocrystals. A supersaturation of the gold droplet may be observed only if:

$$a_{Si} = P_{Si}/P^*_{Si} > 1$$

P_{Si} is the vapor pressure of Si in the gaseous phase and P^*_{Si} is the vapor pressure of pure solid silicon. If we take into account the gaseous species Si_2, Si_3... present in the gaseous phase, the silicon activity may be expressed by:

$$a_{Si} = P_{Si}/P^*_{Si} = \left(P_{Si_2}/P^*_{Si_2}\right)^{1/2} = \left(P_{Si_3}/P^*_{Si_3}\right)^{1/3}$$

The experimental observation of the nanowires growth means that the liquid gold is actually supersaturated with silicon in order to provide $a_{Si} > 1$ in the droplets. The only source of supersaturation is the gaseous phase in which the partial pressure of SiO must be higher than that calculated in the hypothesis of an equilibrium Si/SiO_2 (cristobalite). Experimental evidence leads to the consideration that SiO_2 deposited on the wafer is not under the form of stable cristobalite, but rather under the form of a vitreous, metastable state.

5. SiO_2 Growth and XRD Analysis

Silicon dioxide (SiO_2) is a fundamental and multipurpose material in electronic device fabrication. It can be grown thermally and also deposited in a variety of processes that satisfy different requirements. Some of the common growth and deposition processes for silicon dioxide have been used in this study as shown below:

Comparison of different silicon dioxide growth/ deposition processes

Deposition	Native (N)	Thermal Dry (TD)	Thermal Wet (TW)	Low Temperature Oxidation (LTO)
Source	Air	Oxygen	Steam	$SiH_4 + O_2$
Temperature	Ambient	1100 °C	1100 °C	450 °C

All samples were also heat treated at high temperature (1350 °C, 4 h, under air) in order to check whether the temperature induces modifications. The samples were characterized with the help of wide angle X-Ray diffraction (XRD) using CuKα_1 radiation. The XRD patterns of silicon oxide coatings (Fig. 7) did not show any crystallized silica. The peaks of silicon (wafer) are observed only for thinner SiO_2 coatings (Native oxide and LTO). Furthermore, there is no evidence for the growth of crystalline silica such as cristobalite, even after annealing 4 h at 1350 °C. Therefore, it can be concluded that, essentially all deposited and thermally grown oxides in semiconductor processing are amorphous.

Thus, the activity of the amorphous silica deposited on the silicon wafer would be higher than 1, the standard state for SiO_2 ($a_{SiO_2} = 1$) being the cristobalite. The partial pressure of SiO developed by the equilibrium [2]:

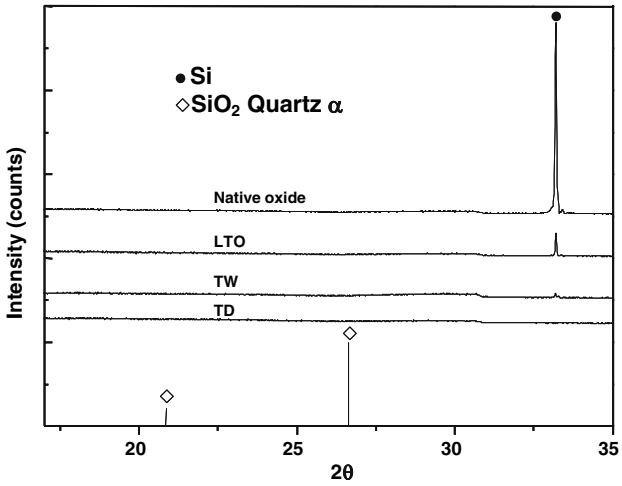

Fig. 7 X-Ray diffraction patterns of silica coating obtained according different methods.

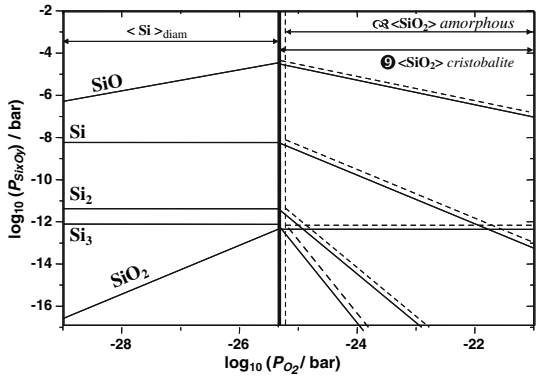

Fig. 8 Relations between the partial pressure of gaseous species and the imposed oxygen potential at 1100 °C.

$$P_{SiO} = K_2\sqrt{a_{Si}a_{SiO_2}}$$

would be higher above the Si/SiO_2 (amorphous) couple than above the Si/SiO_2 (cristobalite) couple. Figure 8 allows comparison of partial pressures of gaseous species at 1100 °C above Si (diamond), SiO_2 (cristobalite) shown in full lines and above SiO_2 (amorphous), shown in dashed lines. The gaseous species taken into account are Si, Si_2, Si_3, SiO, and SiO_2. Although Si_2O_2 was reported to exist, its partial pressure at 1100 °C must be lower than 10^{-21}bar and its accepted entropy of formation, shown in Table 3, seems very improbable. The partial pressure of SiO, which is the main gaseous species, increases above Si according to the reaction $2 <Si> + O_2 \rightarrow 2SiO$ and decreases above SiO_2 according to the reaction $2SiO + O_2 \rightarrow 2<SiO_2>$. The pressure of SiO is raised to a maximum when Si is in equilibrium with SiO_2 and this maximum is higher when SiO_2 is in an amorphous state (dashed line). Indeed, under the conditions of nanowires growth, $a_{Si} = 1$ because Si is the silicon of the wafer and $a_{SiO_2} > 1$ because SiO_2 is amorphous. The oxygen potential is imposed by the equilibrium Si/SiO_2 (amorphous). Actually, the oxygen

Table 3 Thermodynamic data of the Si-O system

$\langle$**Si, dia**$\rangle + \mathbf{O_2} \rightarrow \langle \mathbf{SiO_2}$**, cris**$\rangle$
$\Delta_r G^\circ = -919766.1 - 18.47311T \ln T + 312.2972T + 3.914622 \times 10^{-3} T^2 + 1.757408 \times 10^{-7} T^3 + 1500184\, T^{-1}$ $(523 - 2500\ \text{K})$
$(\text{Si}) + \text{O}_2 \rightarrow (\text{SiO}_2, \text{am})$
$\Delta_r G^\circ = -948511.4 + 3.654347\, T \ln T + 186.1946\, T - 1.078958 \times 10^{-2}\, T^2 + 1.599919 \times 10^{-6}\, T^3 - 84659.19 T^{-1} - 2.0931 \times 10^{-21}\, T^7$ $(273 - 1478\ \text{K})$
$\langle \text{Si, dia} \rangle + \text{O}_2 \rightarrow (\text{SiO}_2, \text{am})$
$\Delta_r G^\circ = -897815 + 3.654347\, T \ln T + 156.0952\, T - 1.078958 \times 10^{-2}\, T^2 + 1.599919 \times 10^{-6}\, T^3 - 84659.19\, T^{-1}$ $(273 - 1478\ \text{K})$
$2\langle \text{Si} \rangle + \text{O}_2 \rightarrow 2\text{SiO(Gas)}$
$\Delta_r G^\circ = -201151.5 - 5.995964T \ln T - 220.2407T + 4.414109 \times 10^{-3} T^2 + 1.599919 \times 10^{-6} T^3 + 560917.6 T^{-1}$ $(800 - 3400\ \text{K})$
$2\langle \text{Si} \rangle + \text{O}_2 \rightarrow \text{Si}_2\text{O}_2\text{(Gas)}$
$\Delta_r G^\circ = -54093 + 304.49\, T$ $(1073 - 1687\ \text{K})$
$2\text{H}_2 + \text{O}_2 \rightarrow 2\text{H}_2\text{O(Gas)}$
$\Delta_r G^\circ = -509118 - 9.145T \ln T + 187.084T$ $(700 - 1700\ \text{K})$

potential is buffered by hydrogen, which reacts with oxygen and gives water vapor according to the reaction:

$$2\text{H}_2 + \text{O}_2 \rightarrow 2\text{H}_2\text{O} \quad [3] \qquad P_{H_2O}/P_{H_2} = \sqrt{K_3 P_{O_2}}$$

At 1100 °C, $K_3 = 1.116 \times 10^{13}$ and $P_{O_2} = 5.73 \times 10^{-21}$ Pa at the Si/SiO_2 (amorphous) equilibrium. As a consequence, the ratio $H_2O/H_2 = 8 \times 10^{-7}$. If the hydrogen content of the Ar-H_2 atmosphere is fixed at 3%, the water content at equilibrium is 25 ppb, which corresponds to a water partial pressure of 2.5 mPa.

Gaseous SiO above the wafer, stable with respect to the Si/SiO_2 (amorphous) mixture, is thus metastable with respect to the Si/SiO_2 (cristobalite) mixture, and the reaction [2] will naturally proceed towards the decomposition of SiO. Without gold droplets, Si and SiO_2 (cristobalite) will germinate on the wafer. The gold droplets acting as a catalyst, SiO will decompose on the surface of the droplet and silicon will dissolve until the liquid-gas equilibrium is reached. When the liquid is in equilibrium with the gaseous phase but supersaturated in silicon with respect to the wafer, the precipitation of silicon nanowires will be observed. For the same reason, the oxygen potential of the gaseous phase being higher than that observed at equilibrium Si/SiO_2 (cristobalite), the silicon nanowires will be oxidized according to the reaction [1] and the result will be a Si/SiO_2 composite nanowire.

6. Discussion

Our model contradicts the traditional explanation of a parasitic oxidation of the SiNW once the protective atmosphere is removed at room temperature. However, it is possible to synthesize SiNW, for instance by decomposition of silanes, without any parasitic oxidation. The model becomes quite credible if we calculate the actual pressure of SiO at equilibrium Si/SiO_2 (amorphous) and if we show that it is sensibly higher than the P_{SiO} calculated from the equilibrium Si/SiO_2 (cristobalite). The data given in Table 3 present, for stable equilibria between Si and O, numerical expressions calculated to give the best fit with experimental ones. The thermodynamic description of liquid silica may be extrapolated toward low temperatures, down to 1480 K (1207 °C), which, according to Golcewski et al.[33] is T_g, the glassy transition temperature of amorphous silica. Below 1480 K, undercooled liquid silica becomes amorphous. The activity of amorphous silica on the silicon wafer is thus given by:

$$a_{\text{SiO2,am}} = \exp\left(\frac{G^\circ_{\text{SiO}_2,\text{am}} - G^\circ_{\text{SiO}_2,\text{cris}}}{RT}\right) = 1.267 \quad \text{at } 1100\,^\circ\text{C}$$

The vapor pressure of SiO is calculated from the equilibrium [2]

$$P_{\text{SiO}} = K_2 \sqrt{a_{\text{Si}} a_{\text{SiO}_2}} = 4.562 \text{ Pa at } 1100^\circ\text{C}$$

where the equilibrium constant K_2 is also the pressure of SiO at equilibrium Si/SiO_2 (cristobalite), which is 4.05 Pa at 1100 °C. The increase of pressure observed when replacing cristobalite by amorphous silica is the order of 13%. That increase seems not very important, but its effect on the chemical potential of Si in the gaseous phase is spectacular.

The decomposition of metastable SiO needs two steps, the first one being the breaking of the Si=O bonding, and the second one, the condensation of gaseous Si.[31,32] Between the two steps, Si exists in the gaseous phase under a potential higher than Si gaseous in equilibrium with the solid and this excess of chemical potential is enough to trigger the nanowires' crystallization.

From the thermodynamic point of view, the Solid-Liquid-Solid (SLS) mechanism involved in the growth of silicon nanowires is shown to be the net result of two consecutive reactions. The production of SiO by reacting an amorphous SiO_2 coating with the silicon of the wafer followed by the disproportionation reaction $2\,\text{SiO} \rightarrow \text{SiO}_2 + \text{Si}$ resulting in the formation of $Si\text{-}SiO_2$ nanowires.

To conclude this study, we consider that the term SVLS seems more appropriate to describe growth of nanowires than the term SLS often cited in the literature, because it takes into account the important role of the SiO species in the gaseous phase. Based on a consistent thermodynamic description of the metastable equilibria in the Si-O-Au system, we pointed out for the first time the source of the driving force needed for the growth of nanowires.

References

1. C.N.R. Rao, F.L. Deepak, G. Gundiah, and A. Govindaraj, Inorganic Nanowires, *Progress Solid State Chem.*, 2003, **31**, p 5-147
2. M.K. Sunkara, S. Sharma, R. Miranda, G. Lian, and E.C. Dickey, Bulk Synthesis of Silicon Nanowires using a Low-Temperature Vapor-Liquid-Solid Method, *Appl. Phys. Lett*, 2001, **79**(10), p 1546-1548
3. J. Su, G. Cui, M. Gherasimova, H. Tsukamoto, J. Han, D. Ciuparu, S. Lim, L. Pfefferle, Y. He, A.V. Nurmikko, C. Broadbridge, and A. Lehman, Catalytic Growth of Group III-Nitride Nanowires and Nanostructures by Metal-Organic Chemical Vapor Deposition, *Appl. Phys. Lett.*, 2005, **86**(013105), p 1546-1548
4. G.S. Park, W.B. Choi, J.M. Kim, Y.C. Choi, Y.H. Lee, and C.B. Lim, Structural Investigation of Gallium Oxide (β-Ga2O3) Nanowires Grown by Arc-discharge, *J. Cryst. Growth*, 2000, **220**, p 494-500
5. A.M. Morales and C.M. Lieber, A Laser Ablation Method for the Synthesis of Crystalline Semiconductor Nanowires, *Science*, 1998, **279**, p 208-211
6. T. Hanrath and B.A. Korgel, Supercritical Fluid-Liquid-Solid (SFLS) Synthesis of Si and Ge Nanowires Seeded by Colloidal Metal Nanocrystals, *Adv. Mater.*, 2003, **15**(5), p 437-440
7. R.S. Wagner and W.C. Ellis, Vapor-Liquid-Solid Mechanism of Single Crystal Growth, *Appl. Phys. Lett*, 1964, **4**(5), p 89-90
8. H.F. Yan, Y.J. Xing, Q.L. Hang, D.P. Yu, Y.P. Wang, J. Xu, Z.H. Xi, and S.Q. Feng, Growth of Amorphous Silicon Nanowires Via a Solid-Liquid-Solid Mechanism, *Chem. Phys. Lett*, 2000, **323**, p 224-228
9. D.P. Yu, Y.J. Xing, Q.L. Hang, H.F. Yan, J. Xu, Z.H. Xi, and S.Q. Feng, Controlled Growth of Oriented Amorphous Silicon Nanowires via a Solid-Liquid-Solid (SLS) Mechanism, *Phys. E*, 2001, **9**, p 305-309
10. M. Paulose, O.K. Varghese, and C.A. Grimes, Synthesis of Gold-Silica Composite Nanowires through Solid-Liquid-Solid Phase Growth, *J. Nanosci. Nanotech.*, 2003, **3**, p 4
11. S.M. Prokes and S. Arnold, Stress-driven formation of Si nanowires, *Appl. Phys. Lett.*, 2005, **86**(193105), p 86-88
12. E. de Vasconcelos, F. dos Santos, E. da Silvas, and H. Boudinov, Nanowires Growth on Si Wafers by Oxygen Implantation and Annealing, *Appl. Surf. Sci.*, 2006, **252**, p 5572-5574
13. H. Okamoto and T.B. Massalski, The Au-Si (Gold-Silicon) System, *Bull. Alloy Phase Diag.*, 1983, **4**(2), p 190-198
14. T. Tanaka and S. Hara, Thermodynamic Evaluation of Binary Phase Diagrams of Small Particle Systems, *Z. Metallkde*, 2001, **92**(5), p 467-472
15. A.T. Dinsdale, SGTE Data for Pure Elements, *Calphad*, 1991, **15**(4), p 317-425
16. N. Saunders, Phase Diagrams Calculations for eight Glass-forming Alloys Systems, *Calphad*, 1985, **9**(4), p 297-309
17. B.K. Teo, Doing Chemistry on Low-dimensional Silicon Surfaces: Silicon Nanowires as Platform and Templates, *Coord. Chem. Rev.*, 2003, **246**, p 229-246
18. E.S. Tankins, Thermodynamic Properties of Dilute Solutions of Oxygen in Liquid Cu-Au Alloys, *Met. Trans.*, 1971, **2**(11), p 3245-3247
19. H.A. Wriedt, The O-Si (Oxygen-Silicon) System, *Bull. Alloy Phase Diag.*, 1991, **11**(1), p 43-61, (Review with 247 references)
20. E.A. Gulbransen and S.A. Jansson, The High Temperature Oxidation, Reduction and Volatilization Reactions of Silicon and Silicon Carbides, *Oxidation of Metals*, 1972, **4**(3), p 181-201
21. B. Hallstedt, Thermodynamic Assessment of the Silicon-Oxygen System, *Calphad*, 1992, **16**(1), p 53-61
22. S.M. Schunurre, J. Gröber, and R. Schmid-Fetzer, Thermodynamics and Phase Stability in the Si-O system, *J. Non-Cryst. Solids*, 2004, **336**, p 1-25
23. K.A. Jackson, A Note on the Si-O Phase Diagram, *Bull. Alloy Phase Diag.*, 1988, **9**(5), p 548-549
24. G. Hollinger, Y. Jugnet, and T.M. Duc, Effect of Heat Treatment on Chemical and Electronic Structure of Solid SiO: An Electron Spectroscopy Study, *Solid State Commun.*, 1977, **21**, p 277-280
25. P. Rocabois, C. Chatillon, and C. Bernard, Vapour Pressure and Evaporation Coefficient of SiO (amorphous) and SiO_2 +Si Mixtures by the Multiple Knudsen Mass Spectrometric Method. Rev, *Int. Hautes Temp. Réfractaires*, 1992-1993, **28**(1), p 37-48
26. C. Chatillon, P. Rocabois, and C. Bernard, High Temperature Analysis of the Thermal Degradation of Silicon-Based Materials. I: Binary Si-O, Si-C and Si-N Compounds, *High Temperatures, High Pressures*, 1999, **31**, p 413-432
27. R.A. Swalin, *Thermodynamics of Solids*. John Wiley, New York, 1962
28. K.S. Yeum, R. Speiser, and D.R. Poirier, Estimation of the Surface Tension of Binary Liquid Alloys, *Metall. Trans.*, 1989, **B20**, p 693-703
29. Z. Jian, K. Kuribayashi, and W. Jie, Solid-Liquid Interface Energy of Metals at Melting Point and Supercooled State, *Mater. Trans*, 2002, **43**(4), p 721-726
30. L.T. Kang, Z.Y. Qiao, B.Y. Yuan, and Z.M. Cao, Calculation of Interfacial Tension based on Sublattice Model and Thermodynamic data, *Calphad*, 2003, **27**(1), p 57-64
31. D. Bahloul-Hourlier, B. Doucey, P. Goursat, and E. Laborde, Investigations on Thermal Reactivity of Si/C/N Nanopowders Produced by Laser Aerosol or Gas Interactions, *J. Mater. Chem*, 2001, **11**, p 2028-2034
32. J. Latournerie, P. Dempsey, J.P. Bonnet, and D. Bahloul-Hourlier, Silicon Oxycarbide Glasses: Part 1- Thermochemical stability, *J. Am. Ceram. Soc.*, 2006, **89**(5), p 1485-1491
33. J.A. Golcewski, H.J. Seifert, and F. Aldinger, A Thermodynamic Model of Amorphous Silicates, *Calphad*, 1998, **22**(3), p 381-396